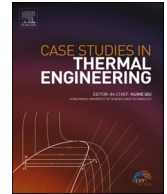




ELSEVIER

Contents lists available at ScienceDirect

## Case Studies in Thermal Engineering

journal homepage: [www.elsevier.com/locate/csite](http://www.elsevier.com/locate/csite)

# Heat and momentum diffusion of ternary hybrid nanoparticles in a channel with dissimilar permeability's and moving porous walls: A Multi-linear regression

Se-Jin Yook<sup>a,1</sup>, C.S.K. Raju<sup>a</sup>, Bander Almutairi<sup>b</sup>, S.U. Mamatha<sup>c</sup>, Nehad Ali Shah<sup>d,1</sup>, Sayed M. Eldin<sup>e,\*</sup>

<sup>a</sup> School of Mechanical Engineering, Hanyang University, 222 Wangsimni-ro, Seongdong-gu, Seoul, 04763, Republic of Korea

<sup>b</sup> Department of Mathematics, College of Sciences, King Saud University, P.O.Box 2455, Riyadh, 11451, Saudi Arabia

<sup>c</sup> Department of Mathematics, Kristu Jayati College (Autonomous), Bangalore, Karnataka, India

<sup>d</sup> Department of Mechanical Engineering, Sejong University, Seoul, 05006, South Korea

<sup>e</sup> Center of Research, Faculty of Engineering, Future University in Egypt, New Cairo, 11835, Egypt

## ARTICLE INFO

Handling Editor: Huihe Qiu

## Keywords:

Ternary hybrid nanofluid  
Wu's slip  
Porous channel  
Convective heat transfer  
Thermal radiation

## ABSTRACT

In recent times, the term Hybrid nanofluid is frequently used owing to its extraordinary influence on different science and engineering processes like therapeutic process, motorized investigational and electrical circuits where energy transference is significant and marine engineering etc. The objective of the present investigation is to supervise the heat and momentum diffusion of ternary hybrid nanoparticles in a channel with dissimilar permeability's and moving porous walls which enables the nanofluid to enter or exist during successive expansion or contractions. In this model, newly proposed Wu's slip circumstance is enforced on the down permeable wall of the channel and analyzed along with thermal radiation and convective heating. The flow and heat diffusion of ternary hybrid flow-1 (Carbon Nanotubes(CNT), Graphene, Aluminum oxide), ternary hybrid flow-2 (Copper oxide, Copper, magnetite), ternary hybrid nanofluid 3 (Paraffin wax, Sand, AA7072 aluminum alloy) water as base fluid is compared and analyzed. The unsteady Navier Stokes equations is converted to partial differential equation by via stream function and the vorticity equation further similarity conversions are used to convert the prevailing flow quantities into non-linear differential equations and then elucidated numerically by shooting procedure with Runge-Kutta (R-K 4th order). Linear Regression method (LRM) is used to model the solution for the flow variables. Outcomes obtained for axial velocity  $f'(\chi)$  and temperature circulation  $\theta(\chi)$  are interpreted by the graph. Achieved outcomes are compared with existing studies. The topmost result of this investigation is found to be -The higher distribution of heat transmission rate is observed in Case-3 (Paraffin wax + Sand + AA7072) with rise in  $Bi_i$ . Since the particles interaction is higher. The second order slip is shown lesser friction in the Copper oxide + copper + magnetite compared to rest of the situations

\* Corresponding author.

E-mail addresses: [ysjnuri@hanyang.ac.kr](mailto:ysjnuri@hanyang.ac.kr) (S.-J. Yook), [cskraju@hanyang.ac.kr](mailto:cskraju@hanyang.ac.kr) (C.S.K. Raju), [baalmutairi@ksu.edu.sa](mailto:baalmutairi@ksu.edu.sa) (B. Almutairi), [mamathasupadhya@gmail.com](mailto:mamathasupadhya@gmail.com) (S.U. Mamatha), [nehadali199@sejong.ac.kr](mailto:nehadali199@sejong.ac.kr) (N.A. Shah), [sayed.eldin22@fue.edu.eg](mailto:sayed.eldin22@fue.edu.eg) (S.M. Eldin).

<sup>1</sup> These authors contributed equally to this work and are co-first authors.

<https://doi.org/10.1016/j.csite.2023.103133>

Received 17 April 2023; Received in revised form 23 May 2023; Accepted 25 May 2023

Available online 26 May 2023

2214-157X/© 2023 Published by Elsevier Ltd.

This is an open access article under the CC BY-NC-ND license

(<http://creativecommons.org/licenses/by-nc-nd/4.0/>).

## 1. Introduction

Studies associated to the laminar fluid flow in permeable walls has continually received the attention owing to their relevance in the technological and biological applications. Which include aerospace engineering, binary gas diffusion, combustion in rocket motors, coolant circulation, filtration, synthetic response in designing, binary gas diffusion, ablation cooling, air circulation in respiratory system, in transportation of biological fluid thru expanding/contracting vessels, synchronic pulsation of porous diaphragms' etc. The exploration towards steady viscous incompressible flow across the rectangular permeable channel was initiated by Berman [1], he considered oblique velocity constituent to be self-regulating of streamwise coordinates and converted resulting Navier Stokes equation to nonlinear single 4th order ODEs with corresponding boundary situations which included permeation Reynolds number ( $R$ ) Since then, numerous theoretical studies dealing with flow and heat transportation in channel with permeable walls was made. Recently, Hatami et al. [2] applied least square and Galerkin method to simulate heat and flow transfer between two parallel plates and they reported Nusselt number improves with the improvement in Reynolds number and volume fraction of nanoparticles. Basir et al. [3] examined chemical reaction in a channel flow considering unsteady nanofluid with contacting/expanding walls and noticed with increase in Reynold number upper channel wall exhibits better heat transfer rate compared with lower wall. Jirawattanapanit et al. [4] analyzed melting rate enhancement inside a thermal energy storage system of finned heat pipe with nano-enhanced phase change material. Rashidi et al. [5] analyzed numerically and analytically two-dimensional (2D) viscous fluid flow between contracting/expanding permeable plates. Khan et al. [6] took up comparative study on hybrid nanofluid flow in semi-infinite channel with expanding/contracting porous walls and observed for positive values of the wall contraction velocity of the fluid increases. Abderrehmane et al. [7] stated hybrid nanofluid mixed convection heat transfer with entropy generation and magnetic effects in porous wall and cylinder. Pandit and Sharma [8] applied wavelet collocation method to oversee the impact in unsteady nanofluid flow through asymmetric porous channel. Sun et al. [9] analyzed temporal stability for the laminar incompressible fluid flow in a porous channel with moving walls and found that in case of wall contraction cross flow  $R$  (Reynolds number) increases. Vijayalakshmi and Srinivas [10] observed near the walls axial velocity declines with improvement in Darcy number in asymmetric flow of nanofluid with thermal radiation permeable channel.

The interest towards dissolving nanoparticles in conventional heat transfer fluid is not a novel idea, anymore. Yet, the work is motivating and stimulating while new fluids are involved. Considering huge significance for the thermal energy and on other side lessening biosphere possessions and ecological apprehensions has provoked by the investigators to the growth of further well-organized temperature transmission liquids by raised temperature transfer proportions. "Hybrid nanofluid" might be ready by melting conflicting nanoparticles as specific components or by softening nanocomposite elements in a convectional functioning liquid. The combination of the nanoparticles is twisted with better Van Der Waals forces and Brownian effort than their particular disgusting strength this recovers atom thickness and steadiness through a period which is beneficial for real-world uses of temperature transmission. The combination of nanoparticles was primarily scrutinized by Bahiraei et al. [11]. Ranga Babu et al. [12] examined challenges and uses related with the combination of nanofluids. Newly, Zhang et al. [13] considered mixture of nanofluid flow over a spinning unsteady disk and perceived development in thermal possessions. Waqas et al. [14] examined mix of nanoparticles considering the melting impact heat transmission and Non-Fourier flux in a rocket needle of the locomotive. Qureshi et al. [15] discovered the heat transition impact on mixture of nanofluids in a parallel channel. In modern eras, captivated by the uses/physical and biochemical possessions of nanoparticles investigators have introduced in discovering flow possessions of the colloidal mix convective flow with three kinds of particles, referend as ternary hybrid nanofluid. Later, Sahu and Kumar [16] experimental study, Sang et al. [17] discussed the synergistic effect of combination of 3 type of nanoparticles, Sahu et al. [18] described the particle nature (shape) has important impact in combination of nanoparticles. Ramesh et al. [19] examined Flow of hybrid CNTs past a rotating sphere subjected to thermal radiation and thermophoretic particle deposition. Newly, Raju et al. [20] scrutinized nonlinear axisymmetric flow considering radiation in expanding/contracting permeable walls filled with ternary particles. Researchers [21–26] examined flow possessions of combination of nanoparticles has tendency to control the flow phenomena, due to this they considered with numerous effects and structures.

In no-slip conditions, the momentum of the flow is zero at fluid-solid crossing point. That means constituent parts and the frame has the similar momentum. Non-Slip condition exhibit impractical in circumstances such as extrusion of polymer dissolves via a tube, when fluid is particulate like liquids, polyethylene industries, foams and interruptions. Also, MEMS and NEMS no slip assumption is not applicable owing to the micro scale dimension of the devices. In addition, it is also observed that fluid offering slip boundary conditions has vital application in biomedical and technological fields such as in exclusive lubricating, refrigeration equipment, ophthalmic coatings, internal cavities, refining in non-natural heart controller, etc. Navier [27] initiated the occurrence of slip circumstances. In which the constituent of the watery momentum peripheral to the border walls is relative to peripheral strain. In literature, one can find significant number of studies and its application considering Navier first-order slip conditions. Recently, Wu [28] proposed the model of 2nd order slip velocity this is useable for the random Kundsens number. This novel model has been recently applied by Alamri et al. [29] to analyze convective radiative Poiseuille nanofluid flow via porous medium considering second order slip. They observed extra sensitivity in velocity for 2nd order slip matched to 1st order slip. Khan et al. [30] studied nanofluid free convection with the 2nd order slip and noticed improvement in 1st and 2nd order slip momentum has declined the thermal and associated boundary layer thickness. Obalalu et al. [31] studied effect of variable electrical conductivity with 1st and 2nd order slip on Casson non-Darcian flow filled with nanoparticles. Hussain et al. [32] investigated porosity and combined magnetic influence on time dependent nano tangent hyperbolic fluid with second order slip they noticed improvement in second order slip maximizes the flow speed. Li et al. [33] studied non-linear reaction and radiation on Maxwell nanofluid unsteady flow considering Wu slip and noticed that velocity reduced with second order slip. Ganesh et al. [34] analyzed Darcy Forchheimer nanofluid flow in a porous medium

considering second order slip over a shrinking/stretching surface. Tulu et al. [35] reported 2nd order slip influence on convection flow due to stretching surface. Very recently, the authors [36–40] are considered the various slip impact with various geometries and found that slip has tendency to control the flow pattern.

Motivated by the above stated investigations, in this study we have extended the works of Raju et al. [20] by incorporating newly proposed Wu’s slip condition on the down permeable wall of the channel. To the best of our knowledge no one studied this 2nd order slip condition (Wu’s slip). Along with we also compared and analyzed thermal radiation and convective heating on the flow and heat transmission of ternary nanofluid 1 (CNT (Carbon nanotubes), Graphene, Aluminum oxide), ternary nanofluid 2 (Copper oxide, Copper, magnetite), ternary hybrid nanofluid 3 (Paraffin wax, Sand, AA7072 aluminum alloy) considering water as base fluid.

### 2. Problem formulation

In this study, incompressible, isothermal, laminar hybrid nanofluid flow bounded by two porous walls which allow the fluid to enter or exit through successive expansion or contraction is considered. One side of the cross section represent the distance  $2(a(t))$  between the walls and it is much smaller compared with width and length of channel. The channel is presumed to be semi-infinite in length. The permeabilities of both the walls are considered to be dissimilar and contact or expand uniformly at a time dependent rate  $\dot{a}(t)$ . Coordinate arrangement is deliberated in a way that the origin  $\hat{x} = 0$  is at the midpoint of the channel. The axial ( $u$ ) and normal ( $v$ ) momentum mechanisms are along the  $x$  and  $y$  directions. In Fig. 1 planar segment of the flow domain is portrayed. With these suppositions and succeeding Raju et al. [20] and Sultan et al. [29] the flow governing equations are:

$$\frac{\partial v}{\partial y} + \frac{\partial u}{\partial x} = 0 \tag{1}$$

$$(\rho_{Thnf}) \left( \frac{\partial u}{\partial t} + u \frac{\partial u}{\partial x} + v \frac{\partial u}{\partial y} \right) = \left( -\frac{\partial p}{\partial x} \right) - (\mu_{Thnf}) \left[ \left( \frac{\varphi u}{K} \right) - \left( \frac{\partial^2 u}{\partial x^2} + \frac{\partial^2 u}{\partial y^2} \right) \right] \tag{2}$$

$$(\rho_{Thnf}) \left( \frac{\partial v}{\partial t} + u \frac{\partial v}{\partial x} + v \frac{\partial v}{\partial y} \right) = \left( -\frac{\partial p}{\partial y} \right) - (\mu_{Thnf}) \left[ \left( \frac{\varphi v}{K} \right) - \left( \frac{\partial^2 v}{\partial x^2} + \frac{\partial^2 v}{\partial y^2} \right) \right] \tag{3}$$

$$(\rho C_p)_{Thnf} \left( \frac{\partial T}{\partial t} + v \frac{\partial T}{\partial x} + u \frac{\partial T}{\partial y} \right) = (k_{Thnf}) \left( \frac{\partial^2 T}{\partial y^2} \right) - \left( \frac{\partial q_R}{\partial y} \right) \tag{4}$$

Related boundary circumstances are:

$$at\ y = - (a(t)),\ u = -u_{slip},\ v = -(v_0) = (-A_0)\dot{a},\ (k_{Thnf}) \frac{\partial T}{\partial y} = (-h_f)(T_1 - T) \tag{5}$$

$$at\ y = (a(t)),\ u = 0,\ v = (-v_1) = (-A_1)\dot{a},\ T = T_0 \tag{6}$$

$$u_{slip} = \left( \frac{2}{3} \right) \left( \frac{3 - l^2 \varepsilon}{\varepsilon} - \left( \frac{1 - l^2}{K_n} \right) \frac{3}{2} \right) \left( \gamma \frac{\partial u}{\partial y} \right) - \left( l^4 + (1 - l^2) \frac{2}{K_n^2} \right) \left( \gamma^2 \frac{\partial^2 u}{\partial y^2} \right) \tag{7}$$

Here,  $l = \min\left(\frac{1}{K_n}, 1\right)$ ,  $0 \leq l \leq 1$ ,  $\varepsilon$ -the momentum accommodation coefficient  $0 \leq \varepsilon \leq 1$ ,  $0.001 \leq K_n \leq 0.1$ ,  $K_n$  Knudsen number,  $\gamma$  the molecular mean free path.  $\Phi$  the permeability of the porous,  $T$  the temperature of the fluid,  $p$  the dimensional pressure,  $t$  is time,  $K$

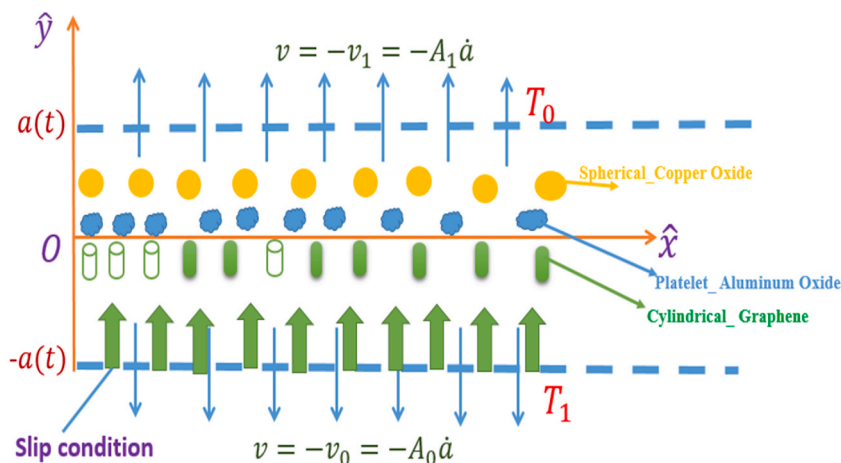


Fig. 1. 2D flow with the expansion and contraction of walls.

the specific permeability,  $T_1$  lower wall temperature and  $T_0$  upper wall temperature,  $A_0 = \frac{y_0}{a}$  and  $A_1 = \frac{y_1}{a}$  the measures of wall permeability,  $h_f$  heat transfer coefficient, and  $\mu_{T_{hnf}}, (\rho C_p)_{T_{hnf}}, \rho_{T_{hnf}}, k_{T_{hnf}}$  represents dynamic viscosity, heat capacitance, density, thermal conductivity of the ternary hybrid nanofluid.  $\Phi_1, \Phi_2$  and  $\Phi_3$  signifies volume of cylindrical, spherical and platelet nanoparticles and  $\Phi = \Phi_1 + \Phi_2 + \Phi_3$  signifies complete volume fractions of nanoparticles. Referring, the combination of particles (cylindrical, spherical and platelet shapes) thermal conductivity and viscosity are

$$\mu_{T_{hnf}} = \frac{(\mu_{nf1})\Phi_1 + (\mu_{nf2})\Phi_2 + (\mu_{nf3})\Phi_3}{\Phi} \tag{8}$$

$$k_{T_{hnf}} = \frac{(k_{nf1})\Phi_1 + (k_{nf2})\Phi_2 + (k_{nf3})\Phi_3}{\Phi} \tag{9}$$

The density ( $\rho_{T_{hnf}}$ ) and heat capacity (Kalidasan et al. [26]) of TF(ternary fluid) (sphere-shaped, platelet and cylindrical shape of solid particles) is given by (Nizar et al. [23], Takabi and Salehi [25], Ho et al. [24]),

$$\rho_{T_{hnf}} = ((\rho_{bf})(1 - \Phi_1 - \Phi_2 - \Phi_3)) + (\Phi_1\rho_{sp1}) + (\Phi_2\rho_{sp2}) + (\Phi_3\rho_{sp3}) \tag{10}$$

$$(\rho C_p)_{T_{hnf}} = \Phi_1(\rho C_p)_{sp1} + \Phi_2(\rho C_p)_{sp2} + \Phi_3(\rho C_p)_{sp3} + (1 - \Phi_1 - \Phi_2 - \Phi_3)(\rho C_p)_{bf} \tag{11}$$

Viscosity and the thermal conductivity of spherical nanoparticle:

$$\mu_{nf1} = (\mu_{bf})(1 + (2.5)\Phi + (6.2)\Phi^2) \tag{12}$$

$$\frac{k_{nf1}}{k_{bf}} = \frac{[k_{sp1} - (2)\Phi(k_{bf} - k_{sp1}) + (2)k_{bf}]}{[k_{sp1} + \Phi(k_{bf} - k_{sp1}) + (2)k_{bf}]} \tag{13}$$

Viscosity and the thermal conductivity of cylindrical nanoparticles:

$$\mu_{nf2} = (\mu_{bf})(1 + (13.5)\Phi + (904.4)\Phi^2) \tag{14}$$

$$\frac{k_{nf2}}{k_{bf}} = \frac{[k_{sp2} - (3.9)\Phi(k_{bf} - k_{sp2}) + (3.9)k_{bf}]}{[k_{sp2} + \Phi(k_{bf} - k_{sp2}) + (3.9)k_{bf}]} \tag{15}$$

Viscosity and thermal conductivity for platelet nanoparticles is:

$$\mu_{nf3} = (\mu_{bf})(1 + (37.1)\Phi + (612.6)\Phi^2) \tag{16}$$

$$\frac{k_{nf3}}{k_{bf}} = \frac{[k_{sp3} - (4.7)\Phi(k_{bf} - k_{sp3}) + (4.7)k_{bf}]}{[k_{sp3} + \Phi(k_{bf} - k_{sp3}) + (4.7)k_{bf}]} \tag{17}$$

Roseland estimates for thermal radiation is employed to abridge the radiative heat flux ( $q_R$ ).

$$q_R = -\frac{4}{3k^*} \nabla(\sigma^* T^4) \tag{18}$$

Here,  $\sigma^*$  Stefan -Boltzmann constants,  $k^*$  signifies mean absorption coefficients.

$T$  is expressed in the form of far field temperature ( $T_0$ ) via Taylor's expansion as:

$$T^4 = T_0^4 + 4(T - T_0)T_0^3 + 6(T - T_0)^2 T_0^2 + \dots \tag{19}$$

Assuming, temperature variations within the flow is minimal and referring Walter's lamma, disregarding square and the higher order terms of  $(T - T_0)$ , Eq. (19) is reduced to

$$T^4 = (T_0^3)(4T - 3T_0) \tag{20}$$

Thus, Eq. (18) turns out to be  $q_R = -\frac{16\sigma^* T_0^3}{3k^*} \frac{\partial T}{\partial y}$ .

The temperature circulation of the ternary solid particles in the channel could be considered as

$$T = \theta(y)B\left(\frac{x}{a}\right)^{p_1} + T_0 \tag{21}$$

$p_1$  power law index of temperature and  $B$  is the fluid constant.

Considering, stream function, flow quantities defined as:

$$\psi = \frac{\nu x f(\chi, t)}{a}, v = (-\nu a^{-1})f(\chi, t), u = \left(\frac{\nu x}{a^2}\right)f_\chi(\chi, t) \tag{22}$$

Where  $f_\chi = \left(\frac{\partial f}{\partial \chi}\right), \chi = \left(\frac{y}{a}\right)$ , and  $\theta(\chi) = \frac{T-T_0}{T_1-T_0}$ .

Substituting Eq. (22) in (1), (2), (3) and (4) and removing the pressure term in momentum equation, subsequent expression is attained.

$$\frac{d^4 f}{d\chi^4} + \left(\frac{N_{T1}}{N_{T2}}\right) R f(\chi) \frac{d^3 f}{d\chi^3} + \left(\frac{N_{T1}}{N_{T2}}\right) (\Lambda) \left[ 3 \frac{d^2 f}{d\chi^2} + \chi \frac{d^3 f}{d\chi^3} \right] - \left[ \left(\frac{N_{T1}}{N_{T2}}\right) (R) \frac{df}{d\chi} \frac{d^2 f}{d\chi^2} + \frac{1}{Da} \frac{d^2 f}{d\chi^2} \right] = 0 \tag{23}$$

$$\left[ \frac{N_{k3}}{N_{k4}} + \frac{4}{3} \frac{Nr}{A_4} \right] \frac{d^2 \theta}{d\chi^2} + (Pr)(R) \left[ \left(\frac{\Lambda}{R}\right) \left( \chi \frac{d\theta}{d\chi} + p_1 \theta(\chi) \right) - (p_1) \frac{df}{d\chi} \theta(\chi) + f(\chi) \frac{d\theta}{d\chi} \right] = 0 \tag{24}$$

and the boundary circumstances are

$$f'(-1) = \lambda f''(-1) + \delta f'''(-1), f(-1) = A_0, \left(\frac{k_{mf}}{k_f}\right) \frac{d\theta(-1)}{d\chi} = -Bi(1 - \theta(-1)) \tag{25}$$

$$\theta(1) = 0, f(1) = A_1, f'(1) = 0$$

In the above equations,

$$N_{T1} = \bar{B}_1 \Phi_1 + \bar{B}_2 \Phi_2 + \bar{B}_3 \Phi_3$$

$$N_{T2} = (1 - \Phi_3 - \Phi_2 - \Phi_1) + \left( \Phi_1 \frac{\rho_{sp1}}{\rho_{bf}} + \Phi_2 \frac{\rho_{sp2}}{\rho_{bf}} + \Phi_3 \frac{\rho_{sp3}}{\rho_{bf}} \right)$$

$$N_{k3} = \bar{B}_4 \Phi_1 + \bar{B}_5 \Phi_2 + \bar{B}_6 \Phi_3$$

$$N_{k4} = (1 - \Phi_3 - \Phi_2 - \Phi_1) + \Phi_1 \left( \frac{(\rho c_p)_{sp1}}{(\rho c_p)_{bf}} \right) + \Phi_2 \left( \frac{(\rho c_p)_{sp2}}{(\rho c_p)_{bf}} \right) + \Phi_3 \left( \frac{(\rho c_p)_{sp3}}{(\rho c_p)_{bf}} \right)$$

$$\bar{B}_1 - 1 = (2.5)\Phi + (6.2)\Phi^2$$

$$\bar{B}_2 - 1 = (13.5)\Phi + (904.4)\Phi^2$$

$$\bar{B}_3 - 1 = (37.1)\Phi + (612.6)\Phi^2$$

$$\bar{B}_4 = \frac{k_{sp1} - (2)\Phi(k_{bf} - k_{sp1}) + (2)k_{bf}}{k_{sp1} + \Phi(k_{bf} - k_{sp1}) + (2)k_{bf}}, \bar{B}_5 = \frac{k_{sp2} - (3.9)\Phi(k_{bf} - k_{sp2}) + (3.9)k_{bf}}{k_{sp2} + \Phi(k_{bf} - k_{sp2}) + (3.9)k_{bf}}$$

$$\bar{B}_6 = \frac{k_{sp3} - (4.7)\Phi(k_{bf} - k_{sp3}) + (4.7)k_{bf}}{k_{sp3} + \Phi(k_{bf} - k_{sp3}) + (4.7)k_{bf}}$$

$R = \left(\frac{uv}{\nu}\right)$  is Reynolds number,  $R < 0$  is injection and  $R > 0$  is the suction,  $\Lambda(t) = \left(\frac{aa}{\nu}\right)$  is wall expansion ratio and  $\Lambda(t) > 0$  is for the expansion and  $\Lambda(t) < 0$  for the contraction,  $\lambda = \left(\frac{-2}{3}\right) \left(\frac{3-l^2 \epsilon}{\epsilon} - \left(\frac{1-l^2}{K_n}\right) \frac{3}{2}\right) \left(\frac{l}{a}\right)$  is first order slip velocity,  $\delta = \left(l^4 + (1-l^2) \frac{2}{K_n^2}\right) \left(\frac{l^2}{4a^2}\right)$  is second order slip velocity,  $Pr = \frac{\mu_f (Cp)_f}{k_f}$  Prandtl number,  $Da = \left(\frac{K}{\rho a^2}\right)$  is Darcy number,  $Nr = \left(\frac{4\sigma T_0^3}{kk_f}\right)$  the thermal radiation parameter,  $Bi = \left(\frac{h_f a}{k_f}\right)$  Biot number,

Referring Vijayalakshmi et al. [ 10] and Raju et al. [ 20] dimensionless shear stress and Nusselt number at the wall is considered as:

$$\tau = \left( \frac{x}{(1 - \Phi_1 - \Phi_2 - \Phi_3)^{2.5}} \right) (f''(\chi))_{\chi=-1,1} \tag{26}$$

$$Nu = \left( \frac{-k_{mf}}{k_f} \right) \frac{\partial T}{\partial \chi} = \left( -\frac{k_{Tmf}}{k_f} \right) \theta'(\chi)_{\chi=(-1,1)} \tag{27}$$

### 3. Multi-linear statistics of regression

In the regression line  $\mathbb{R} = A_1 X_1 + A_2 X_2 + B, \dots, A_1, A_2, \dots$  are the slope of regression,  $X_1, X_2, \dots$  are an independent property. Here there three cases of nanoparticles considered. Case3: Paraffin Wax-Spherical shape + Sand-Cylindrical shape + AA7072-Platelet shape-magenta; Case-2: CNT-Spherical shape + Graphene-Cylindrical shape + Aluminum Oxide-Platelet Shape-Green; Case-2: Copper oxide(Spherical)+Copper (Cylindrical)+ fe3o4 (Platelet)-Blue color.

Multi-linear regression equation for the friction factor coefficient is

$$\begin{aligned}
 cf\_lw\_parafin &= 2794.226299 + 924.7019484 * \lambda - 8.729398779 * \delta - 35350.78379 * \Phi + 0 * \Phi_1 + 54662.90211 * \Phi_2 + 0 * \Phi_3 \\
 &- 1354.443981 * Da; \\
 cf\_lw\_cnt &= 181.2356134 + 46.56846521 * \lambda - 8.901511806 * \delta - 1788.06663 * \Phi + 0 * \Phi_1 + 613.7107275 * \Phi_2 + 0 * \Phi_3 \\
 &- 54.27335732 * Da; \\
 cf\_lw\_copper &= 268.831231 + 72.046915512 * \lambda - 303.3464775 * \delta - 716.60887802 * \Phi + 0 * \Phi_1 - 3613.997822 * \Phi_2 + 0 * \Phi_3 \\
 &+ 50.71441252 * Da; \\
 cf\_up\_copper &= -24363.2134 + 52021.70031 * \lambda + 1772.027929 * \delta + 139756.3219 * \Phi + 0 * \Phi_1 - 191943.8498 * \Phi_2 + 0 * \Phi_3 \\
 &+ 26965.79174 * Da; \\
 cf\_up\_parafin &= -24761.2 + 49289.06 * \lambda + 1372.14 * \delta + 154159.7 * \Phi + 0 * \Phi_1 - 215838 * \Phi_2 + 0 * \Phi_3 + 26555.26 * Da; \\
 cf\_up\_cnt &= -19180.93205 + 40956.45452 * \lambda + 1128.237851 * \delta + 111562.7318 * \Phi + 0 * \Phi_1 - 153738.6627 * \Phi_2 + 0 * \Phi_3 \\
 &+ 21258.06087 * Da;
 \end{aligned}$$

Multi-linear regression equation for the rate of heat transfer is

$$\begin{aligned}
 nu\_parafin &= 0 * Bi - 0.757423356 * R + 0.350212259 * Nr + 0 * \lambda + 17.73329167 * \Phi + 0.272803523; \\
 nu\_copper &= 0 * Bi - 4.897145997 * R - 0.884736123 * Nr + 0 * \lambda + 885.0513611 * \Phi - 51.49727289; \\
 nu\_cnt &= 0 * Bi - 1.50533789814815 * R - 0.105616074 * Nr + 0 * \lambda + 17.43641667 * \Phi + 4.625699565.
 \end{aligned}$$

#### 4. Interpretation of outcomes

The R-K method with boundary circumstances is used to elucidate the terms of ODEs (23)–(25). For the simulating results the impact of dimensionless factors like  $Bi, \lambda, \delta, Da$  and  $Nr$  on temperature and velocity fields. The numerical explanations were considered in this analysis for various parameter values as  $\Phi_3 = 0.05, A_1 = -0.2, Pr = 6.2, Da = 0.5, \lambda = 0.1, \delta = 0.1, R = 2, Nr = 0.3, p1 = 1, \Phi = 0.05, \Lambda = 2, \Phi_1 = 0.05, \Phi_2 = 0.05$ . During this exploration, these values are conserved as constant.

##### 4.1. Multiple parameter skin friction coefficient and local Nusselt number

By taking the help of Table 1 and Table 2 the 3D graphs designed all three circumstances of hybrid flow combinations for skin friction and rate of heat transmission at both the lower and upper plates. These plots shown from Fig. 2(a, b, c) and 3(a, b, c). The  $Bi$  vs  $\Phi$  &  $\Phi$  vs  $Nr$  is plotted in Fig. 2(a) and (b). The rate of heat transfer is better in Case-2 equated to Case-1 and Case-3. The  $Bi, Re$  &  $Bi, \lambda$  variation on  $Nus$  is plotted in Fig. 2(c) and found that the linear impact *w.r.t* all the cases, whereas the Case-2 distribution is more compared to remaining solid particle mixture. Similarly, in Fig. 3(a) the  $\lambda$  vs  $\delta$  on friction at both plates for all hybrid mixture is plotted and found that the upper plate has higher distribution of heat transfer rate compared to lower plate in all three cases of hybrid mixture. The moderately related performance is witnessed in Fig. 3(b) and (c) for all the three cases of solid particles. It displays the  $\lambda$  vs  $Da$  and  $\lambda$  vs  $\Phi$  on friction at both plates for all hybrid mixtures and identified that the Case-2 has lesser friction at the plates equated with other two cases of the flow.

In Table 3 listed the physical possessions of solid particles, for instance  $\rho, \rho_{cp}$  and  $k$  of base fluid, beside with the several types and environments of nano particles. The authentication present outcomes with accessible works under limited circumstance  $\Lambda = -1, R = 1, Pr = 6.2, P1 = 1, Nr = 1, Da = 0.5$  is demonstrated in Table-6. Table 7 shows the statistical validation of the considered model with all compositions of mixtures. All the measures are 1 it means 100% these parameters are influences the flow pattern and considered model is positively 100% correct and error value is 0%.

##### 4.2. Momentum and temperature distributions

The Green, Red and Blue colour lines characterize the three dissimilar situations for ternary hybrid solid nanoparticles correspondingly. The Green (CNT + Graphene + Alumium oxide)-Spherical, cylindrical and platelet respectively), Red (Copper Oxide-Spherical + Copper-cylindrical + ferrous oxide-platelet) and Blue (Paraffin Wax + Sand + AA7072- Spherical, cylindrical and platelet respectively) color lines describes the case-1, case-2 and case-3 respectively.

Fig. 4, 5(a, b), 6(a, b), 7(a, b) and 8 display the variations of the  $f'(\chi), \theta(\chi)$  outlines for changing values of  $Bi, \lambda, \delta, Da$  and  $Nr$  correspondingly for all three cases of solid particles mixture. Similarly, the Tables-4 and 5 displayed the impact of friction factor and heat transfer rate for all three cases of the flow. Fig. 4 displays  $Bi$  variation on  $\theta(\chi)$  for all three cases of solid particles mixtures.  $Bi$  improves the temperature in all cases of solid mixtures this help us get opposite behavior in the local Nusselt number. It is interesting to know that thermal field of Case-2 has higher distribution equated to Case-1 and Case-3, whereas Case-3 has more  $-\theta'(-1)$  equated with other two situations (From Table-5). The impact of  $\lambda$  variation on  $f'(\chi)$  and  $\theta(\chi)$  shown in Fig. 5(a) and (b). The  $f'(\chi)$  is shown mixed sense and is  $\theta(\chi)$  shown improvement as  $\lambda$  raises, whereas from Table-4 & 5 the friction and local Nusselt number is reduced in all

**Table 1**  
Multi-linear regression data of Nusselt number is given as for various governing parameters.

$Bi$	$R$	$Nr$	$\Lambda$	$\Phi$	$Nus$		
					Case-1	Case-2	Case-3
0.1	3	5	0.5	0.09	1.347591	1.150883	9.042231
0.2	5	1	0.8	0.072	-1.8873	-1.75118	-13.144041
0.3	7	1.5	1.1	0.122	-2.34038	-3.94285	20.871867
0.4	9	2	1.4	0.1	-4.07025	-7.38993	-8.835923

**Table 2**  
Multi-linear regression data for the friction factor coefficient for all three compositions.

$\lambda$	$\delta$	$\Phi = \begin{pmatrix} \Phi_1 \\ +\Phi_2 \\ +\Phi_3 \end{pmatrix}$	Friction factor						
			$Da$	Paraffin wax mixture		CNT mixture		Copper mixture	
				Lower plate	Upper plate	Lower plate	Upper plate	Lower plate	Upper plate
0.1	-0.1	0.6	0.2	10.301232	-8.535433	609.728864	-605.114228	4.245257	-2.587006
0.2	0.1	0.09	0.4	1988.090721	-1061.6476	37.709352	-19.880289	27.99705	-14.477369
0	0.2	0.072	0.6	90.512423	-44.217139	25.515028	-12.795222	143.6268	-70.203792
-0.1	0.3	0.122	0.8	35.931583	-18.724518	-56.968965	-7.937307	-56.932	-8.062878
-0.2	0.4	0.1	0	-0.014893	-22323.474	-0.012265	-18378.212	-0.01558	-23346.156
0.3	0.5	0.103	-0.2	25.007663	-16.084056	21.12147	-12.959546	33.13449	-20.609634
0.4	-0.5	0.12	-0.4	14.784337	-13.008373	17.59221	-15.552329	306.9044	-375.54381

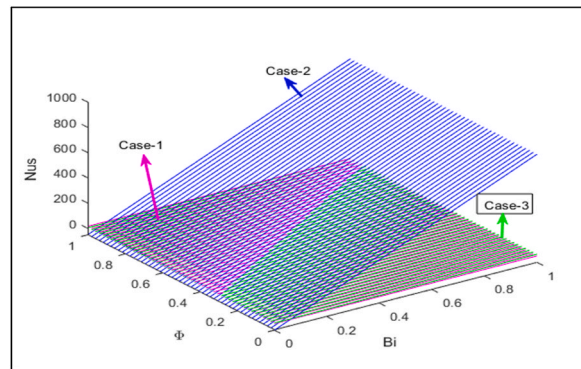


Fig. 2(a).  $Bi$  &  $\Phi$  variation on  $Nus$ .

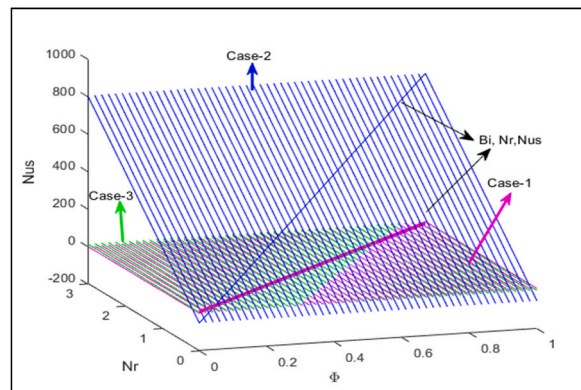


Fig. 2(b).  $Nr$  &  $\Phi$  variation on  $Nus$ .

three situations. Fig. 6(a) and (b) illustrate the effect of  $\delta$  variation on  $f'(\chi)$  and  $\theta(\chi)$  for all the three cases. As  $\delta$  raises encourages the jumps this helps to show mixed sense in the momentum and temperature field, while the friction factor and heat transmission rates are encouraged for all situations (Tables 4 and 5). The impact of Darcy on velocity and thermal fields is shown in Fig. 7(a) and (b) for three situations. Initially encouragement and decrement phenomena observed in all situations whereas this results are matched with the Raju et al. [20] and Vijayalakshmi and Srinivas [10]. From Tables 4 and 5 found that the reduction rate in both the friction factor and heat transfer rate for all situations. Fig. 8 displays the influence of  $Nr$  on  $\theta(\chi)$ . It observed that rising the intensity of radiation discharges more temperature, causing in a growth in the  $\theta(\chi)$  and it help to lessen the friction factor and rate of heat transmission for all the situations., this results matches with the Raju et al. [20] and Vijayalakshmi and Srinivas [10].

**5. Conclusion**

In this report, the dynamics of Second order slip on axisymmetric hybrid flow in a contracting and expanding Darcy convectively

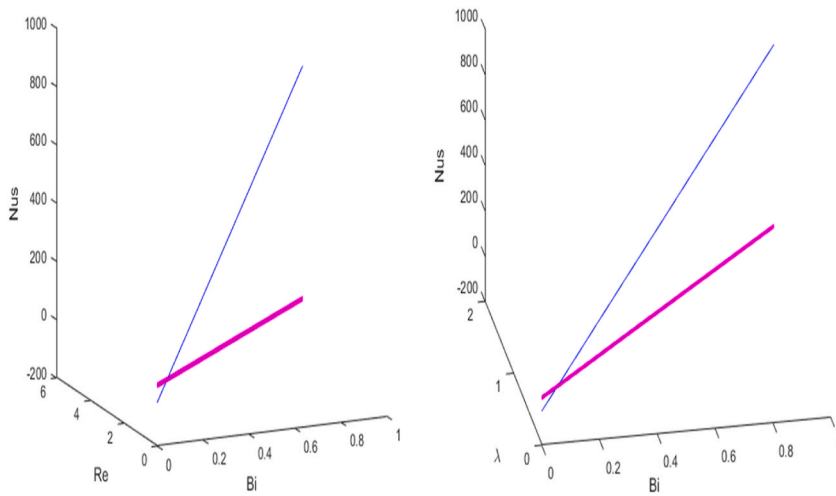


Fig. 2(c).  $Bi$ ,  $Re$  &  $Bi$ ,  $\lambda$  variation on  $Nus$ .

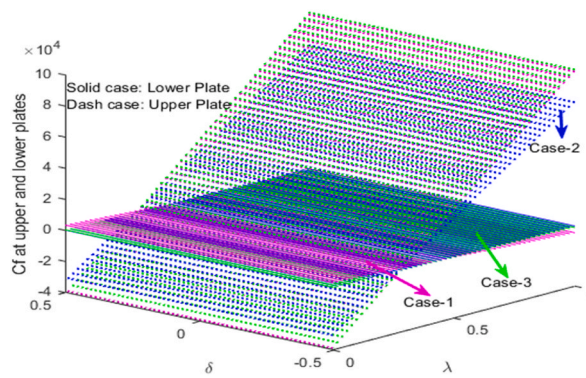


Fig. 3(a).  $\lambda$  &  $\delta$  variation on  $Cf$ .

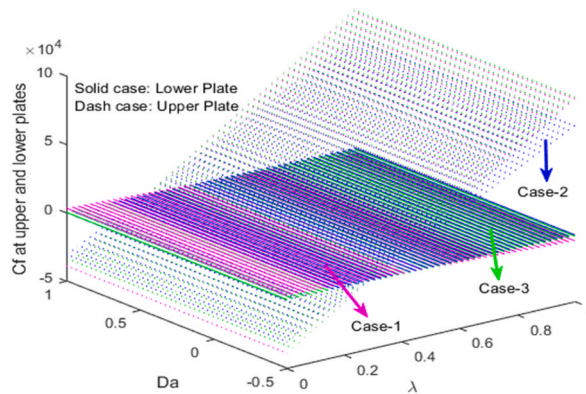


Fig. 3(b).  $\lambda$  &  $Da$  variation on  $Cf$ .

heated walls: Nonlinear viscosity and conductivity models. When the thermal conductivity of the three kinds of nanoparticles is small and a different three kinds of nanoparticles are adequately large in magnitude had been explored. Volume fraction of all the three circumstances of nanoparticles are considered as 5% Meanwhile, platelet aluminum oxide, ferrous oxide and AA7072, cylindrical shape graphene, copper and sand, Spherical shape as CNT, Copper oxide and paraffin wax nanoparticles were measured for their thermal conductivity. Depending on the result of the examination and discussion of outcomes, it is worthy to accomplish that.

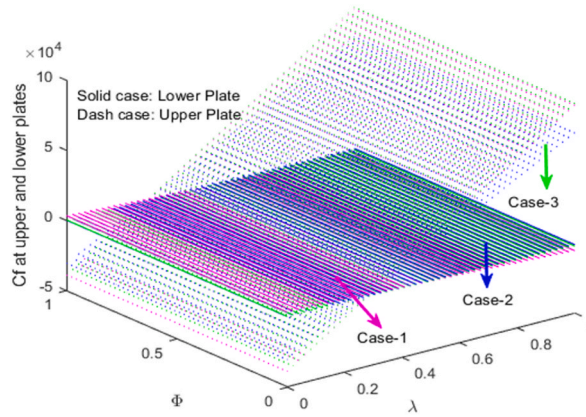


Fig. 3(c).  $\lambda$  and  $\Phi$  deviation on  $C_f$ .

**Table 3**  
Thermo-physical possessions of nano and base fluids.

Nanofluid properties	Density $\rho \left(\frac{kg}{m^3}\right)$	Heat capacitance $C_p \left(\frac{J}{kgK}\right)$	Thermal conductivity $k \left(\frac{W}{mK}\right)$	Nanoparticle shapes
Pure H <sub>2</sub> O	997.1	4.179	0.623	Spherical
Paraffin wax	900	2900	0.25	
CNT	5100	410	3007.4	
CuO	6500	535.6	20	Cylindrical
Graphene	2200	790	5000	
(Cu)	8933	385	400	
Sand	26500	730	1.5	Platelet
Al <sub>2</sub> O <sub>3</sub>	3970	765	40	
Magnetite (Fe <sub>3</sub> O <sub>4</sub> )	5200	670	6	
AA7072	2720	893	222	

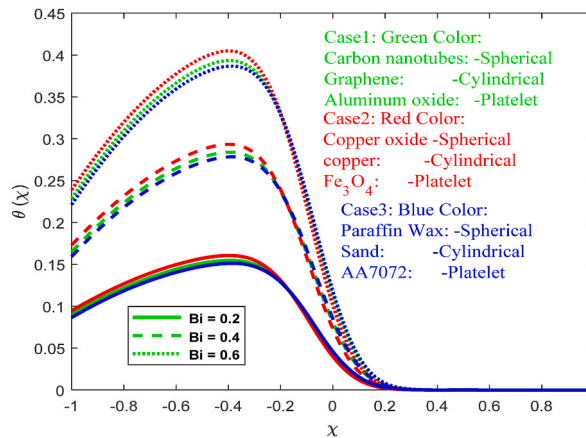


Fig. 4.  $Bi$  deviation on  $\theta(x)$ .

- The rate of heat transfer is better in Case-2 (Copper oxide + copper + magnetite) compared to other two combination of mixtures.
- The higher distribution of heat transfer rate is observed in Case-3 (Paraffin wax + Sand + AA7072) with rise in  $Bi$ , Since the particles interaction is higher.
- The second order slip is shown lesser friction in the Copper oxide + copper + magnetite compared to rest of the situations.
- As the raising values of  $Bi$  vs  $\Phi$  monotonically encourages the Nusselt number.
- The linear relationship observed in  $Bi$  vs  $Re$  and  $Bi$  vs  $\lambda$  in Nusselt number.

**Table 4**  
Numerical values for skin friction  $f''(-1)$  and  $f''(1)$  for various governing parameters.

Bi	$\lambda$	$\delta$	Da	Nr	$f''(-1)$			$f''(1)$		
					Case1	Case2	Case3	Case1	Case2	Case3
0.2					100.853044	91.670783	107.203803	-46.948110	-43.342972	-49.297057
0.4					100.853044	91.670783	107.203803	-46.948110	-43.342972	-49.297057
0.6					100.853044	91.670783	107.203803	-46.948110	-43.342972	-49.297057
	0.2				77.488765	72.530559	80.698510	-40.437276	-37.842105	-42.055511
	0.4				50.919423	49.146224	51.991730	-33.927453	-32.056783	-35.064905
	0.6				37.327697	36.512674	37.806877	-30.900349	-29.271364	-31.886294
		0.1			100.853044	91.670783	107.203803	-46.948110	-43.342972	-49.297057
		0.15			127.521141	109.875823	141.202890	-55.543955	-49.422196	-59.995856
		2			153.658028	126.828999	175.934364	-65.586680	-56.076349	-73.125941
			0.1		214.223313	175.866886	245.395604	-71.614352	-62.659079	-78.447691
			0.15		145.849949	126.467222	160.364446	-57.384902	-51.874850	-61.219497
			2		121.018241	107.563242	130.685026	-51.808201	-47.390238	-54.768456
				1	100.853044	91.670783	107.203803	-46.948110	-43.342972	-49.297057
				3	100.853044	91.670783	107.203803	-46.948110	-43.342972	-49.297057
				5	100.853044	91.670783	107.203803	-46.948110	-43.342972	-49.297057

**Table 5**  
Numerical values for Nusselt number  $-\theta'(-1)$  for various parameters.

Bi	$\lambda$	$\delta$	Da	Nr	$-\theta'(-1)$		
					Case1	Case2	Case3
0.2					-0.194750	-0.192788	-0.151580
0.4					-0.357395	-0.352204	-0.279012
0.6					-0.495269	-0.486222	-0.387642
	0.2				-0.348372	-0.336824	-0.275732
	0.4				-0.472247	-0.448391	-0.378376
	0.6				-0.571423	-0.539541	-0.459566
		0.1			-0.279568	-0.276102	-0.217939
		0.15			-0.224909	-0.232885	-0.169092
		2			-0.185813	-0.200920	-0.135045
			0.1		-0.179885	-0.193497	-0.131254
			0.15		-0.229642	-0.235175	-0.174145
			2		-0.254930	-0.255941	-0.196297
				1	-0.320991	-0.318429	-0.256966
				3	-0.438909	-0.437624	-0.367326
				5	-0.589405	-0.588307	-0.506345

**Table 6**  
Validation of results  $\Lambda = -1, R = 1, Pr = 6.2, P1 = 1, Nr = 1, Da = 0.5$ .

$\chi$	$f(\chi)$			$\theta(\chi)$		
	Current Results	Raju et al. [20]	Vijayalakshmi and Srinivas [10]	Current Results	Raju et al. [20]	Vijayalakshmi and Srinivas [10]
0	0.00000	0.000	0.00000	0.107321	0.107321	0.107322
0.3	0.40630	0.40630	0.40630	0.0493809	0.0493808	0.0493809
0.5	0.65606	0.65606	0.65606	0.0282924	0.0282924	0.0282925
0.7	0.85538	0.85538	0.85538	0.01458	0.01458	0.01458

**Table 7**  
Statistical Validation of Nusselt number in three composition of mixtures.

Regression Statistics	CNT mixture	Copper Mixture	Paraffin Mixture
Multiple R	100%	100%	100%
R Square	100%	100%	100%
Adjusted R Square	65535		
Standard Error	0%		
Observations	4		

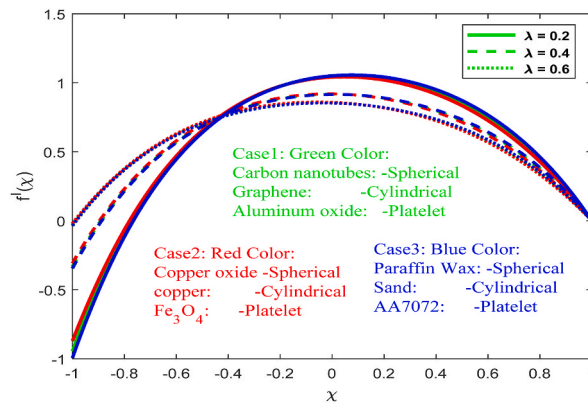


Fig. 5(a).  $\lambda$  variation on  $f'(\chi)$ .

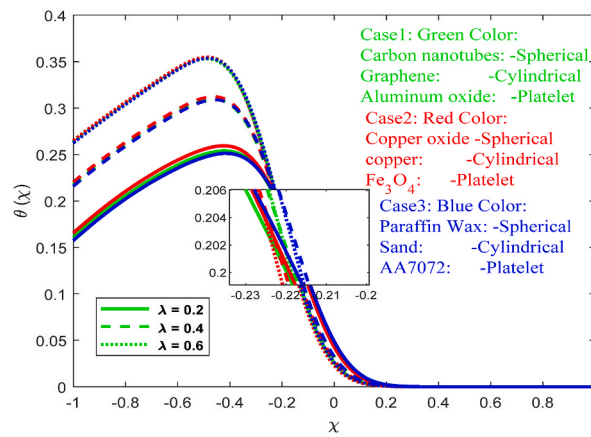


Fig. 5(b).  $\lambda$  deviation on  $\theta(\chi)$ .

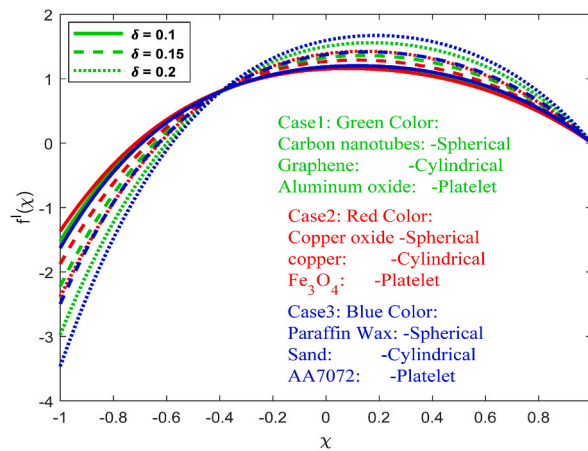


Fig. 6(a).  $\delta$  difference on  $f'(\chi)$ .

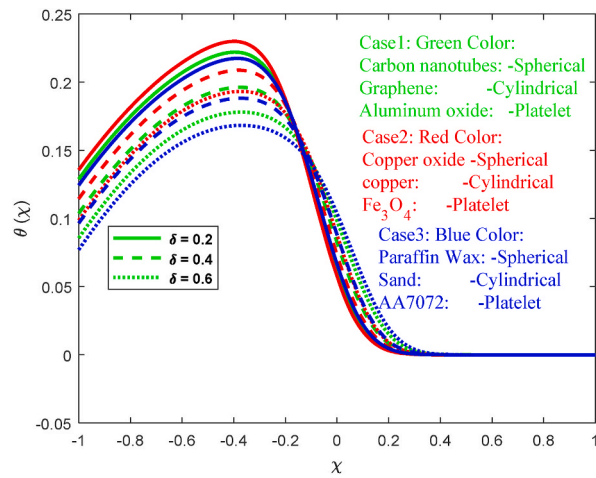


Fig. 6(b).  $\delta$  deviation on  $\theta(\chi)$ .

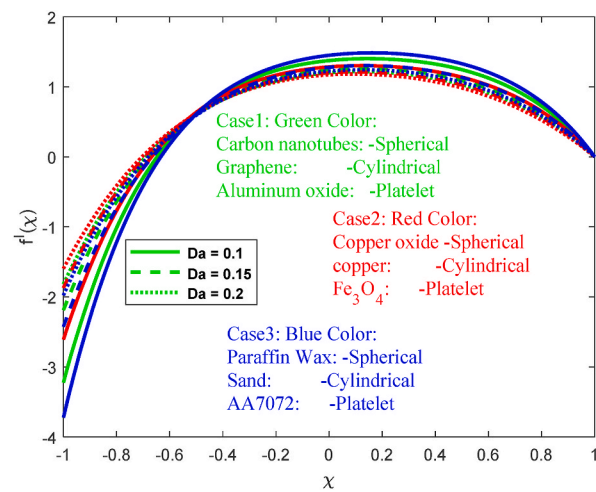


Fig. 7(a).  $Da$  variation on  $f'(\chi)$ .

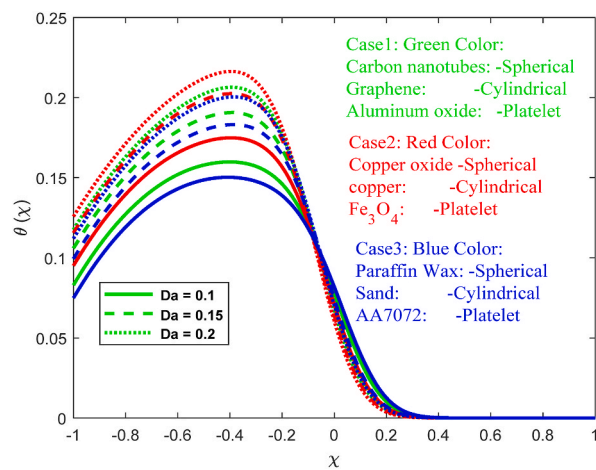


Fig. 7(b).  $Da$  variation on  $\theta(\chi)$ .

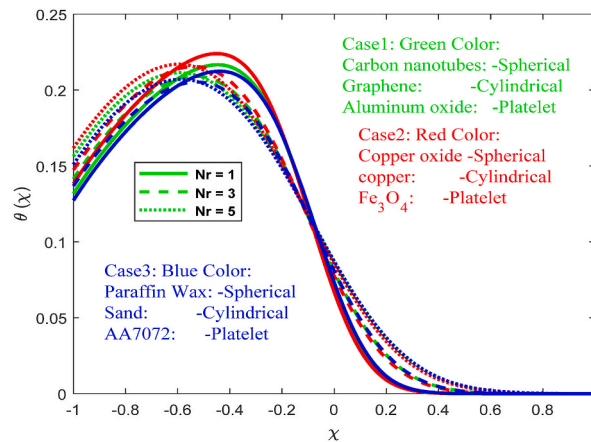


Fig. 8.  $Nr$  variation on  $\theta(x)$ .

### Author statement

All authors contributed equally to this work.

### Declaration of competing interest

The authors have no conflict of interest. All authors are equally collaborated.

### Data availability

Data will be made available on request.

### Acknowledgments

The authors extend their appreciation to King Saud University for funding this research through Researchers Supporting Project number: RSPD2023R650, King Saud University, Riyadh, Saudi Arabia. This work was partially funded by the research center of the Future University in Egypt, 2022.

### References

- [1] A.S. Berman, Laminar flow in channels with porous walls, *J. Appl. Phys.* 24 (9) (1953) 1232–1235.
- [2] M. Hatami, M. Sheikholeslami, D.D. Ganji, Nanofluid flow and heat transfer in an asymmetric porous channel with expanding or contracting wall, *J. Mol. Liq.* 195 (2014) 230–239.
- [3] M.F.M. Basir, K. Naganthran, E. Azhar, Z. Mehmood, S. Mukhopadhyay, R. Nazar, I. Khan, Unsteady nano-bioconvective channel flow with effect of  $n$ th order chemical reaction, *Open Phys.* 18 (1) (2020) 1011–1024.
- [4] A. Jirawattanapanit, A. Abderrahmane, A. Mourad, K. Guedri, O. Younis, B. Bouallegue, K. Subkrajang, G. Rajchakit, N.A. Shah, A numerical investigation of a melting rate enhancement inside a thermal energy storage system of finned heat pipe with nano-enhanced phase change, *Material. Nanomaterials* 12 (15) (2022) 2519.
- [5] M.M. Rashidi, M.A. Sheremet, M. Sadri, S. Mishra, P.K. Pattnaik, F. Rabiei, E. Erfani, Semi-analytical solution of two-dimensional viscous flow through expanding/contracting gaps with permeable walls, *Math. Comput. Appl.* 26 (2) (2021) 41.
- [6] N. Khan, K. Al-Khaled, A. Khan, M.S. Hashmi, S.U. Khan, M.I. Khan, S. Qayyum, Aspects of constructive/destructive chemical reactions for viscous fluid flow between deformable wall channel with absorption and generation features, *Int. Commun. Heat Mass Tran.* 120 (2021), 104956.
- [7] A. Abderrahmane, N.A.A. Qasem, O. Younis, R. Marzouki, A. Mourad, J.D. Chung, MHD hybrid nanofluid mixed convection heat transfer and entropy generation in a 3-D triangular porous cavity with zigzag wall and rotating cylinder, *Mathematics* 10 (2022) 769.
- [8] S. Pandit, S. Sharma, On the use of wavelets for analysis of nanofluid flow and thermal transmission through asymmetric porous channel, *Proc. Natl. Acad. Sci., India, Sect. A* (2022) 1–13.
- [9] Y. Sun, P. Lin, Z. Guo, Temporal stability of multiple similarity solutions for porous channel flows with expanding or contracting walls, *Phys. Fluids* 33 (8) (2021), 083606.
- [10] A. Vijayalakshmi and S. Srinivas, Asymmetric flow of a nanofluid between expanding or contracting permeable walls with thermal radiation, *Frontiers in Heat and Mass Transfer*, 7(10)92016) 1-11.
- [11] M. Bahiraei, S.M. Hosseinalipour, Experimental study of nanofluid convective heat transfer for implementation of dispersion model considering non-uniform particle distribution, *Exp. Heat Tran.* 27 (2014) 452–471.
- [12] J.A. Ranga Babu, K.K. Kumar, S. Srinivasa Rao, State-of-art review on hybrid nanofluids, *Renew. Sustain. Energy Rev.* 77 (2017) 551–565.
- [13] X.H. Zhang, A. Algehyne, E.G. Alshehri, M. Bilal, M.A. Khan, M. A. T. Muhammad, The parametric study of hybrid nanofluid flow with heat transition characteristics over a fluctuating spinning disk, *PLoS One* 16 (8) (2021), e0254457.
- [14] H. Waqas, T. Muhammad, S. Noreen, U. Farooq, M. Alghamdi, Cattaneo-Christov heat flux and entropy generation on hybrid nanofluid flow in a nozzle of rocket engine with melting heat transfer, *Case Stud. Therm. Eng.* 28 (2021), 101504.
- [15] M.A. Qureshi, S. Hussain, M.A. Sadiq, Numerical simulations of MHD mixed convection of hybrid nanofluid flow in a horizontal channel with cavity: impact on heat transfer and hydrodynamic forces, *Case Stud. Therm. Eng.* 27 (2021), 101321.
- [16] R.R. Sahoo, V. Kumar, Development of a new correlation to determine the viscosity of ternary hybrid nanofluid, *Int. Commun. Heat Mass Tran.* 111 (2020), 104451.

- [17] L. Sang, W. Ai, Y. Wu, C. Ma, Enhanced specific heat and thermal conductivity of ternary carbonate nanofluids with carbon nanotubes for solar power applications, *Int. J. Energy Res.* 44 (1) (2020) 334–343.
- [18] M. Sahu, J. Sarkar, Steady-state energetic and exergetic performances of single-phase natural circulation loop with hybrid nanofluids, *J. Heat Tran.* 141 (8) (2019), 082401.
- [19] G. Ramesh, J. Madhukesh, N.A. Shah, S.-J. Yook, Flow of hybrid CNTs past a rotating sphere subjected to thermal radiation and thermophoretic particle deposition, *Alex. Eng. J.* 64 (2022) 969–997.
- [20] C.S.K. Raju, N.A. Ahammad, K. Sajjan, N.A. Shah, S.J. Yook, M.D. Kumar, Nonlinear movements of axisymmetric ternary hybrid nanofluids in a thermally radiated expanding or contracting permeable Darcy Walls with different shapes and densities: simple linear regression, *Int. Commun. Heat Mass Tran.* 135 (2022), 106110.
- [21] M. Sahu, J. Sarkar, Steady-state energetic and energetic performances of single-phase natural circulation loop with hybrid nanofluids, *J. Heat Tran.* 141 (8) (2019), 082401.
- [22] M.Z. Ashraf, S.U. Rehman, S. Farid, A.K. Hussein, B. Ali, N.A. Shah, W. Weera, Insight into significance of bioconvection on MHD tangent hyperbolic nanofluid flow of irregular thickness across a slender elastic surface, *Mathematics* 10 (2022) 2592.
- [23] Nizar Ahammed, Lazarus Godson Asirvatham, Somchai Wongwises, Entropy generation analysis of graphene–alumina hybrid nanofluid in multiport minichannel heat exchanger coupled with thermoelectric cooler, *Int. J. Heat Mass Tran.* 103 (2016) 1084–1097.
- [24] C.J. Ho, J.B. Huang, P.S. Tsai, Y.M. Yang, Preparation and properties of hybrid water-based suspension of Al<sub>2</sub>O<sub>3</sub> nanoparticles and MEPCM particles as functional forced convection fluid, *Int. Commun. Heat Mass Tran.* 37 (5) (2010) 490–494.
- [25] Q. Lou, B. Ali, S.U. Rehman, D. Habib, S. Abdal, N.A. Shah, J.D. Chung, Micropolar dusty fluid: coriolis force effects on dynamics of MHD rotating fluid when lorentz force is significant, *Mathematics* 10 (15) (2022) 2630.
- [26] A. Rauf, N.A. Shah, A. Mushtaq, T. Botmart, Heat transport and magnetohydrodynamic hybrid micropolar ferrofluid flow over a non-linearly stretching sheet, *AIMS Mathematics* 8 (1) (2023) 164–193.
- [27] C.L.M.H. Navier, Mémoire sur les lois du mouvement des fluides, *Mem Acad R Sci Inst France* 6 (1823) 389–440.
- [28] L. Wu, A slip model for rarefied gas flows at arbitrary Knudsen number, *Appl. Phys. Lett.* 93 (25) (2008), 253103.
- [29] S.Z. Alamri, R. Ellahi, N. Shehzad, A. Zeeshan, Convective radiative plane Poiseuille flow of nanofluid through porous medium with slip: an application of Stefan blowing, *J. Mol. Liq.* 273 (2019) 292–304.
- [30] M.I. Khan, F. Alzahrani, Free convection and radiation effects in nanofluid (Silicon dioxide and Molybdenum disulfide) with second order velocity slip, entropy generation, Darcy-Forchheimer porous medium, *Int. J. Hydrogen Energy* 46 (1) (2021) 1362–1369.
- [31] A.M. Obalalu, O.A. Ajala, A. Abdulraheem, A.O. Akindele, The influence of variable electrical conductivity on non-Darcian Casson nanofluid flow with first and second-order slip conditions, *Partial Differential Equations in Applied Mathematics* 4 (2021), 100084.
- [32] S. Hussain, F. Ahmad, H. Ayed, M.Y. Malik, H. Waqas, M.M. Al-Sawalha, S. Hussain, Combined magnetic and porosity effects on flow of time-dependent tangent hyperbolic fluid with nanoparticles and motile gyrotactic microorganism past a wedge with second-order slip, *Case Stud. Therm. Eng.* 26 (2021), 100962.
- [33] Y.X. Li, H. Waqas, K. Al-Khaled, S.A. Khan, M.I. Khan, S.U. Khan, Y.M. Chu, Simultaneous features of Wu's slip, nonlinear thermal radiation and activation energy in unsteady bio-convective flow of Maxwell nanofluid configured by a stretching cylinder, *Chin. J. Phys.* 73 (2021) 462–478.
- [34] N.V. Ganesh, A.A. Hakeem, B. Ganga, Darcy–Forchheimer flow of hydromagnetic nanofluid over a stretching/shrinking sheet in a thermally stratified porous medium with second order slip, viscous and Ohmic dissipations effects, *Ain Shams Eng. J.* 9 (4) (2018) 939–951.
- [35] A. Tulu, W. Ibrahim, Effects of Second-Order Slip Flow and Variable Viscosity on Natural Convection Flow Of/water Hybrid Nanofluids Due to Stretching Surface, *Mathematical Problems in Engineering*, 2021.
- [36] S. Upadhy, SV Siva Rama Raju Mamatha, C.S.K. Raju, N.A. Shah, Jae Dong Chung, Importance of entropy generation on Casson, Micropolar and Hybrid magneto-nanofluids in a suspension of cross diffusion, *Chin. J. Phys.* 77 (2022) 1080–1101.
- [37] P. Priyadarshini, M. Vanitha Archana, N. Ameer Ahammad, C.S.K. Raju, Se-jin Yook, N.A. Shah, Gradient descent machine learning regression for MHD flow: metallurgy process, *Int. Commun. Heat Mass Tran.* 138 (2022), 106307.
- [38] Hu Ge-JiLe, N.A. Shah, Y.M. Mahrous, Pooja Sharma, C.S.K. Raju, S. Mamatha Upddhya, Radiated magnetic flow in a suspension of ferrous nanoparticles over a cone with brownian motion and thermophoresis, *Case Stud. Therm. Eng.* 25 (2021), 100915.
- [39] M. Dinesh Kumar, C.S.K. Raju, Kiran Sajjan, Essam R. El-Zahar, N.A. Shah, Linear and quadratic convection on 3D flow with transpiration and hybrid nanoparticles, *Int. Commun. Heat Mass Tran.* 134 (2022), 105995.
- [40] S.U. Mamatha, RLV Renuka Devi, N. Ameer Ahammad, N.A. Shah, B. Madhusudhan Rao, C.S.K. Raju, M. Ijaz Khan, Kamel Guedri, Multi-linear regression of triple diffusive convectively heated boundary layer flow with suction and injection: lie group transformations, *Int. J. Mod. Phys. B* 37 (1) (2023), 2350007.